



# Measurement of the top quark mass using the matrix element technique in two lepton final states in $p\bar{p}$ collisions at $\sqrt{s} = 1.96$ TeV

The D0 Collaboration  
(Dated: March 18, 2016)

We present a measurement of the top quark mass in  $p\bar{p}$  collisions at a center-of-mass energy 1.96 TeV at the Fermilab Tevatron Collider. The data are collected by the D0 experiment for a total integrated luminosity of  $9.7 \text{ fb}^{-1}$ . The matrix element technique is applied to  $t\bar{t}$  events with two leptons (electrons or muons) and at least two jets. The calibration of the jet energy scale determined in the lepton + jets final state is applied to jet energies. This correction allows a significant reduction of the systematic uncertainty in the measurement. We obtain a top quark mass of  $m_t = 173.9 \pm 1.8 \text{ GeV}$ .

## I. INTRODUCTION

The top quark is the heaviest elementary particle of the standard model (SM) [1–3]. It was discovered in 1995 by the D0 and CDF experiments at the Tevatron  $p\bar{p}$  collider at Fermilab [4, 5] and has several unique features. The top quark mass ( $m_t$ ) is a free parameter of the SM Lagrangian and can not be predicted from first principles. Despite the fact that the top quark decays weakly, its large mass leads to a very short lifetime of  $\approx 5 \cdot 10^{-25} \text{ s}$  [6–8]. It decays to a  $W$  boson and a  $b$  quark before hadronizing, a process that has a characteristic time of  $1/\Lambda_{\text{QCD}} \approx (200 \text{ MeV})^{-1}$  equivalent to  $\tau_{\text{had}} \approx 3.3 \cdot 10^{-24} \text{ s}$ , where  $\Lambda_{\text{QCD}}$  is the fundamental scale of quantum chromodynamics (QCD). This provides a unique possibility to measure the mass of the top quark high precision.

At the Tevatron, top quarks are produced mainly as  $t\bar{t}$  pairs through the strong interaction. At leading order (LO) in perturbative QCD, a pair of top quarks is produced via quark-antiquark ( $q\bar{q}$ ) annihilation with a probability of about 85% [9, 10], or via gluon-gluon (gg) fusion (see Fig. 1).

Final states in  $t\bar{t}$  production are classified according to the decay of the two  $W$  bosons. In this measurement we use events in the dilepton final state where both  $W$  bosons decay to leptons:  $t\bar{t} \rightarrow W^+b W^- \bar{b} \rightarrow \ell\ell'\nu_\ell\nu_{\ell'}b\bar{b}$ . More specifically, we consider the three combinations of leptons,  $ee$ ,  $e\mu$ , and  $\mu\mu$ , including also electrons and muons from leptonic decays of  $\tau$  leptons:  $W \rightarrow \tau\nu_\tau \rightarrow \ell\nu_\ell\nu_\tau$ .

We present an updated measurement of the top quark mass in the dilepton channel using the matrix element (ME) approach. This measurement uses all data accumulated by the D0 experiment during the Run II data taking period

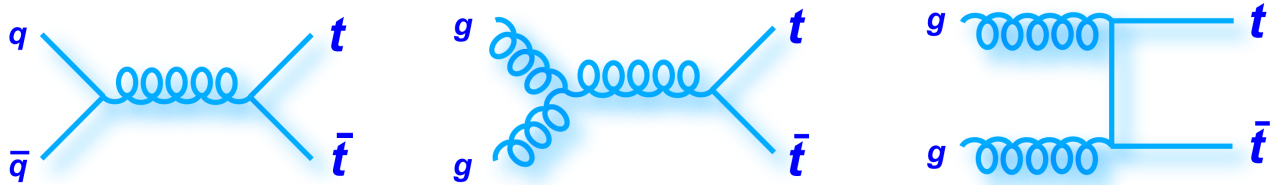


FIG. 1: LO Feynman diagrams for the top quark production.

for an integrated luminosity of  $9.7 \text{ fb}^{-1}$ . Similarly to the recent mass measurement in the dilepton final state using the neutrino weighting technique [11], we correct jet energies by a factor obtained in the top quark mass measurement in the lepton + jets ( $\ell$ +jets) analysis [1, 2]. We also use the final D0 jet energy scale (JES) corrections [12] and the refined corrections of the  $b$ -quark jet energy scale [12].

## II. DETECTOR AND EVENT SAMPLES

### A. Detector and object identification

The D0 detector is described in detail in Refs. [13–19]. It has a central tracking system consisting of a silicon microstrip tracker and a central fiber tracker, both located within a 2 T superconducting solenoidal magnet. The central tracking system is designed to optimize tracking and vertexing at detector pseudorapidities of  $|\eta_{\text{det}}| < 2.5$ <sup>1</sup>. A liquid-argon sampling calorimeter has a central section covering pseudorapidities  $|\eta_{\text{det}}|$  up to  $\approx 1.1$ , and two end calorimeters that extend coverage to  $|\eta_{\text{det}}| \approx 4.2$ , with all three housed in separate cryostats. An outer muon system, with pseudorapidity coverage of  $|\eta_{\text{det}}| < 2$ , consists of a layer of tracking detectors and scintillation trigger counters in front of 1.8 T toroids, followed by two similar layers after the toroids.

Electrons are identified as energy clusters in the calorimeter within a cone of radius  $\mathcal{R} = \sqrt{(\Delta\eta)^2 + (\Delta\phi)^2} = 0.2$  (where  $\phi$  is the azimuthal angle) that are consistent in their longitudinal and transverse profiles with expectations of electromagnetic showers. More than 90% of the energy of an electron candidate must be deposited in the electromagnetic part of the calorimeter. Electrons are required to be isolated by demanding that less than 20% of its energy is deposited in an annulus of  $0.2 < \mathcal{R} < 0.4$  around its direction. This cluster has to be matched to track reconstructed in the central tracking system. We consider electrons in the CC with  $|\eta_{\text{det}}| < 1.1$  and in the EC with  $1.5 < |\eta_{\text{det}}| < 2.5$ . The transverse momenta of electrons ( $p_T^e$ ) must be greater than 15 GeV. In addition, we use an electron multivariate discriminant based on tracking and calorimeter information to reject jets misidentified as electrons. It has between 75% and 80% efficiency to select electrons, and a rejection rate of  $\approx 96\%$  for jets.

Muons are identified [20] as segments in at least one layer of the muon system that are matched to a tracks reconstructed in the central tracking system. Reconstructed muons must have  $p_T > 15$  GeV and satisfy two isolation criteria. First, the transverse energy deposited in the calorimeter annulus around the muon  $0.1 < \mathcal{R} < 0.4$  ( $E_T^{\mu, \text{iso}}$ ) must be less than 15% of the transverse momentum of the muon ( $p_T^\mu$ ). Secondly, the sum of the transverse momenta of the tracks in a cone of radius  $\mathcal{R} = 0.5$  around the muon track in the central tracking system ( $p_T^{\mu, \text{iso}}$ ) must be less than 15% of  $p_T^\mu$ .

Jets are identified as energy clusters in the electromagnetic and hadronic parts of the calorimeter reconstructed using an iterative mid-point cone algorithm with radius  $\mathcal{R} = 0.5$  [21] and  $|\eta_{\text{det}}| < 2.5$ . A jet energy scale (JES) correction is determined by calibrating the energy deposited in the jet cone using transverse momentum balance in photon+jet and dijet events [22].

Additionally, we correct the difference in the single-particle response between data and simulation yielding a parton-flavor dependent JES correction [12]. This correction significantly reduces the bias in the energy and the total JES uncertainty of the jets initiated by  $b$ -quarks. Jets in simulated events are corrected for residual differences in energy resolution and energy scale between data and simulation. These correction factors are measured by comparing data

<sup>1</sup> The pseudorapidity is defined as  $\eta = -\ln[\tan(\theta/2)]$ , where  $\theta$  is the polar angle of a reconstructed particle originating from a primary vertex with respect to the proton beam direction. The detector pseudorapidity  $\eta_{\text{det}}$  is defined relative to a center of the detector instead of the primary vertex.

and simulation in Drell-Yan ( $Z/\gamma^* \rightarrow ee$ ) events with accompanying jets [12]. When a muon track overlaps with the jet cone, the momentum of that muon is added to the jet  $p_T$ , assuming that the muon originates from the semileptonic decay of a hadron belonging to the jet.

The typical JES uncertainty is about 2%. We improve this uncertainty by calibrating the jet energy after event selection with a scale factor  $k_{\text{JES}}$  measured in the lepton+jets final state using jets associated with the  $W$ -boson decay [1, 2]. The  $k_{\text{JES}}$  correction factor is applied to the jet  $p_T$  in data as  $p_T^{\text{corr}} = p_T/k_{\text{JES}}$ , independently for each data taking period. We apply the corrections averaged over  $e$ +jet and  $\mu$ +jet final states (reported in Table 1). The uncertainties related to the determination and propagation of the  $k_{\text{JES}}$  scale factor are accounted for as systematic uncertainties.

Epoch	$k_{\text{JES}}$	Integrated Luminosity
RunIIa	$0.993 \pm 0.016$	$1081 \text{ pb}^{-1}$
RunIIb1	$1.027 \pm 0.013$	$1223 \text{ pb}^{-1}$
RunIIb2	$1.033 \pm 0.008$	$3034 \text{ pb}^{-1}$
RunIIb3 and RunIIb4	$1.026 \pm 0.006$	$4398 \text{ pb}^{-1}$

TABLE 1: The JES correction factor  $k_{\text{JES}}$  and its statistical uncertainty, averaged over  $e$ +jet and  $\mu$ +jet final states, for different data taking periods with their corresponding integrated luminosities.

We use a multivariate analysis (MVA) to identify jets originating from  $b$  quarks [23, 24]. The algorithm combines the information from the impact parameters of tracks and from variables that characterize the properties of secondary vertices within jets. Jet candidates for  $b$  tagging are required to have at least two tracks with  $p_T > 0.5$  GeV originating from the vertex of the  $p\bar{p}$  interaction and, to be matched to a jet reconstructed from the tracks.

The missing transverse momentum (or missing transverse energy),  $\cancel{p}_T$ , is reconstructed from the energy deposited in the calorimeter cells, and corrections to  $p_T$  for leptons and jets are propagated into  $\cancel{p}_T$ . A significance in  $\cancel{p}_T$ ,  $\sigma_{\cancel{p}_T}$ , is defined for each event through a likelihood discriminant constructed from the ratio of  $\cancel{p}_T$  to its uncertainty.

## B. Event selection

The dilepton final state contains two isolated charged leptons, two  $b$ -quark jets and a significant  $\cancel{p}_T$  due to escaping neutrinos. We follow the approach developed in Ref. [25, 26] for the event selection, using the criteria listed below:

- (i) For the  $ee$  and  $\mu\mu$  channels, we select events that pass at least one single-lepton trigger, while for the  $e\mu$  channel, we consider events selected through a mixture of single and multilepton triggers and lepton+jet triggers. Efficiencies for single electron and muon triggers are measured using  $Z/\gamma^* \rightarrow ee$  or  $Z/\gamma^* \rightarrow \mu\mu$  data, and found to be  $\approx 99\%$  and  $\approx 80\%$ , respectively, for dilepton signal events. For the  $e\mu$  channel, the trigger efficiency is  $\approx 100\%$ .
- (ii) We require at least one  $p\bar{p}$  interaction vertex in the interaction region with  $|z| < 60$  cm, where  $z$  is the coordinate along the beam axis, and  $z = 0$  is the center of the detector. At least three tracks with  $p_T > 0.5$  GeV must be associated with this vertex.
- (iii) We require at least two isolated leptons with  $p_T > 15$  GeV, both originating from the same interaction vertex. We consider electrons and muons identified with the standard D0 identification criteria [20, 27] in the pseudorapidity range of  $|\eta_{\text{det}}| < 2.0$  for muons and  $|\eta_{\text{det}}| < 1.1$  or  $1.5 < |\eta_{\text{det}}| < 2.5$  for electrons. The two highest- $p_T$  leptons must have opposite electric charges.
- (iv) To reduce the background from bremsstrahlung in the  $e\mu$  final state, we require the distance in  $(\eta, \phi)$  space between the electron and the muon trajectories to be  $\mathcal{R}(e, \mu) > 0.3$ .
- (v) We require the presence of at least two jets with  $p_T > 20$  GeV and  $|\eta_{\text{det}}| < 2.5$ .
- (vi) The  $t\bar{t}$  final state contains two  $b$ -quark jets.

To improve the separation between signal and background, we apply a selection using the  $b$ -identification MVA discriminant of the two jets of largest  $p_T$ . We use different cutoffs of the MVA variable, corresponding to  $b$ -quark jet identification efficiencies in  $t\bar{t}$  events of 84% in  $e\mu$ , 80% in  $ee$ , 78% in  $\mu\mu$ , with background misidentification efficiencies, of 23%, 12%, 7% respectively. These correspond to the following requirements on MVA discriminant:  $\text{maxMVA} > 0.025$  for  $ee$ ,  $\text{maxMVA} > 0.02$  for  $e\mu$  and  $\text{maxMVA} > 0.075$  for  $\mu\mu$  channel.

- (vii) Additional selection criteria based on global event properties further improve the signal purity. In the  $e\mu$  events, we require  $H_T > 110$  GeV, where  $H_T$  is the scalar sum of the transverse momenta of the leading lepton and the two leading jets. In the  $ee$  final state, we require  $\sigma_{p_T} > 5$ , while in the  $\mu\mu$  channel, we require  $\not{p}_T > 40$  GeV and  $\sigma_{p_T} > 2.5$ .
- (viii) Rarely, the numerical integration of the matrix elements, described in section IV, may yield extremely small probabilities which does not numerically allow any proper use of the event. We reject such events using a selection which has an efficiency of 99.97% for simulated  $t\bar{t}$  signal samples. For background MC events, the efficiency is 99.3%. No event is removed from the final data sample by this requirement.

### C. Simulation of the signal and background events

The main sources of background in the  $\ell\ell$  ( $ee$ ,  $e\mu$ ,  $\mu\mu$ ) channel are the Drell-Yan production  $q\bar{q} \rightarrow Z/\gamma^* \rightarrow \ell\ell$ , diboson production ( $WW$ ,  $WZ$ ,  $ZZ$ ), and instrumental background. The instrumental background arises mainly from ( $W \rightarrow \ell\nu$ )+jets and multijet events in which one or two jets are misidentified as electrons or where muons or electrons originating from semileptonic decays of a heavy-flavor hadron appear as isolated. To estimate the  $t\bar{t}$  signal efficiency and the background contamination, we use Monte Carlo (MC) simulation for all contributions except for the instrumental background, which is estimated from data.

The number of the expected  $t\bar{t}$  signal events is estimated using the tree-level LO matrix element generator ALPGEN (version v2.11) [28] for the hard-scattering process with up to two additional partons, interfaced with the PYTHIA generator [29] (version 6.409, D0 modified tune A [30]) for parton showering and hadronization. The CTEQ6M parton distribution functions [31, 32] are used for the generation, and the top quark mass value is set to 172.5 GeV. The NNLO theoretical cross section of 7.23 pb [33] is used for the normalization. Generated MC events are processed using a GEANT-based [34] simulation of the D0 detector. To simulate effects from additional overlapping  $p\bar{p}$  interactions, “zero bias” events are selected randomly in collider data and overlaid on the simulated events. For the ME method calibration, we use samples with the top quark mass of 165 GeV, 170 GeV, 175 GeV, 180 GeV. Those samples are generated with the same settings as the sample with the mass 172.5 GeV. Drell-Yan samples are simulated using the ALPGEN generator for the hard-scattering process with up to three additional partons, and the PYTHIA generator for parton showering and hadronization. We generated separately events  $Z +$  heavy flavor partons,  $Z \rightarrow b\bar{b}$  and  $Z \rightarrow c\bar{c}$ , and  $Z +$  light flavor partons. The MC cross sections for the heavy flavor samples are scaled-up with the K-factors of 1.52 for  $Z \rightarrow b\bar{b}$  and 1.67 for  $Z \rightarrow c\bar{c}$ . In the diboson events simulation, the PYTHIA generator is used for both the hard-scattering and parton showering parts.

### D. Estimation of the instrumental background contributions

In the  $ee$  and  $e\mu$  channels, we determine the contributions from events with jets misidentified as electrons using the “matrix method” [35]. A loose sample of events ( $n_{\text{loose}}$ ) is defined following the same selection as used for the  $t\bar{t}$  candidate sample in items (i) – (viii) above, but ignoring the requirement on the electron MVA discriminant. For the dielectron channel, we drop the MVA requirement on one of the electrons chosen randomly.

We measure the efficiency  $\varepsilon_e$  that events with a true electron pass the requirement on the electron MVA discriminant using  $Z/\gamma^* \rightarrow ee$  data. We also measure the efficiency  $f_e$  that events with a misidentified jet pass the electron MVA requirement using  $e\mu$  events chosen with selection criteria items (i) – (v), but requiring leptons of the same electric charge. For muons, we also apply a reversed isolation requirement:  $E_T^{\mu,\text{iso}}/p_T^\mu > 0.2$ ,  $p_T^{\mu,\text{iso}}/p_T^\mu > 0.2$ , and  $\not{p}_T < 15$  GeV, to minimize the contribution from  $W \rightarrow e\nu$ +jets events.

We extract the number of events with jets misidentified as electrons ( $n_f$ ), and the number of events with true electrons ( $n_e$ ), by solving the equations:

$$n_{\text{loose}} = n_e/\varepsilon_e + n_f/f_e, \quad (1)$$

$$n_{\text{tight}} = n_e + n_f, \quad (2)$$

where  $n_{\text{tight}}$  is the number of events remaining after implementing the selections (i) – (vii). The factors  $f_e$  and  $\varepsilon_e$  are measured separately for each jet multiplicity (0, 1, and 2 jets), and separately for electron candidates in the central and end parts of the calorimeter. Typical values of  $\varepsilon_e$  are 0.7 – 0.8 in the CC and 0.65 – 0.75 in the EC. Values of  $f_e$  are 0.005 – 0.010 in the CC, and 0.005 – 0.020 in the EC.

Channel	$Z/\gamma^*$	Diboson	Instrumental	$t\bar{t}$	Total	Selected
$e\mu$	$13.0^{+1.7}_{-1.6}$	$3.7^{+0.8}_{-0.8}$	$16.4^{+4.0}_{-4.0}$	$260.6^{+22.5}_{-16.3}$	$293.8^{+23.5}_{-17.7}$	346
$ee$	$13.8^{+2.1}_{-1.9}$	$1.9^{+0.4}_{-0.4}$	$1.8^{+0.2}_{-0.2}$	$88.0^{+9.1}_{-8.2}$	$105.5^{+10.3}_{-9.5}$	104
$\mu\mu$	$10.6^{+1.3}_{-1.4}$	$1.7^{+0.4}_{-0.4}$	0	$76.0^{+6.2}_{-4.1}$	$88.3^{+6.7}_{-4.7}$	92
$\ell\ell$	$37.4^{+5.1}_{-4.9}$	$7.3^{+1.6}_{-1.6}$	$18.2^{+4.0}_{-4.0}$	$424.6^{+37.8}_{-28.6}$	$487.6^{+40.5}_{-31.9}$	545

TABLE 2: Numbers of expected and selected events in data. Systematic uncertainties are shown for expected number of events.

In the  $e\mu$  and  $\mu\mu$  channels, we determine the number of events with an isolated muon arising from decays of hadrons in jets relying on the same selection as for the  $e\mu$  or  $\mu\mu$  channels, but requiring that both leptons have the same charge. In the  $\mu\mu$  channel, the number of events is taken to be the number of same-sign events. In the  $e\mu$  channel, it is the number of events in the same-sign sample after subtracting the contribution from events with jets misidentified as electrons.

To use the ME technique, we additionally need a pool of events from which to calculate probabilities corresponding to the instrumental background. To select these events in the  $e\mu$  channel we use exactly the same selection as for the analysis except for the lepton identification. We require events to satisfy criteria (i)–(vii), but ignoring the requirement on the electron MVA discriminant. Using this selection we obtain a background sample of 2901 events. In the  $\mu\mu$  channel the number of the multijet and  $W$ +jets background events is zero (Table 2). In the  $ee$  channel, the number of such events is non-zero, but small. We do not select any template events for them, but instead increase the number of background events due to  $Z$ -boson production by the corresponding amount in the calibration procedure.

### III. EVENT YIELD AND CONTROL PLOTS

The numbers of predicted background events, as well as the expected numbers of signal events for the final selection in  $e\mu$ ,  $\mu\mu$  and  $ee$  channels are given in Table 2 and show the high signal purity of the selected sample. Comparisons between distributions measured in the data and expectations from simulated samples after the final selection are shown in Figures 2-5 for the combined  $ee$ ,  $e\mu$  and  $\mu\mu$  channels. The jet  $p_T$  and  $H_T$  distributions in Figures 4 and 5 are shown after applying the  $k_{JES}$  correction from the  $\ell$ +jets analysis [1, 2].

### IV. MATRIX ELEMENT TECHNIQUE

In this measurement we use a matrix element (ME) approach [36]. This approach allowed the most precise top quark mass measurement at the Tevatron in the  $\ell$ +jets final state [1, 2] and was used in the previous measurement of  $m_t$  in the  $\ell\ell$  final state using  $5.3 \text{ fb}^{-1}$  [37]. The matrix element method for this analysis is described below.

#### A. Event probability calculation

The ME technique associates to each event a probability calculated as:

$$P(x, f_{t\bar{t}}, m_t) = f_{t\bar{t}} \cdot P_{t\bar{t}}(x, m_t) + (1 - f_{t\bar{t}}) \cdot P_{\text{bkg}}(x), \quad (3)$$

where  $f_{t\bar{t}}$  is the fraction of the  $t\bar{t}$  events in the data set,  $P_{t\bar{t}}(m_t)$  and  $P_{\text{bkg}}$  are the respective per-event probabilities calculated under the hypothesis that the selected event is either a  $t\bar{t}$  event characterized by a top quark mass  $m_t$ , or that is a background event. Here  $x$  represents the set of the measured parameters, i.e.,  $p_T$ ,  $\eta$ , and  $\phi$  for jets and leptons. In this measurement, we assume that the masses of top quark and anti-top quark are the same [38–41]. The probability  $P_{t\bar{t}}(x, m_t)$  is calculated as

$$P_{t\bar{t}}(x, m_t) = \frac{1}{\sigma_{\text{obs}}(m_t)} \int f_{\text{PDF}}(q_1) f_{\text{PDF}}(q_2) \frac{(2\pi)^4 |\mathcal{M}(y, m_t)|^2}{q_1 q_2 s} W(x, y) d\Phi_6 dq_1 dq_2. \quad (4)$$

Here,  $q_1$  and  $q_2$  represent the respective fractions of proton and antiproton momenta carried by the initial state partons,  $f_{\text{PDF}}$  represents the parton distribution functions,  $s$  is the square of the  $p\bar{p}$  center-of-mass energy, and  $y$  refers to partonic final state four-momenta of the particles. The detector transfer functions  $W(x, y)$  correspond to the probability for reconstructing true four-momenta  $y$  as  $x$ . For the ME calculation, the LO matrix element  $\mathcal{M}(y, m_t)$  of

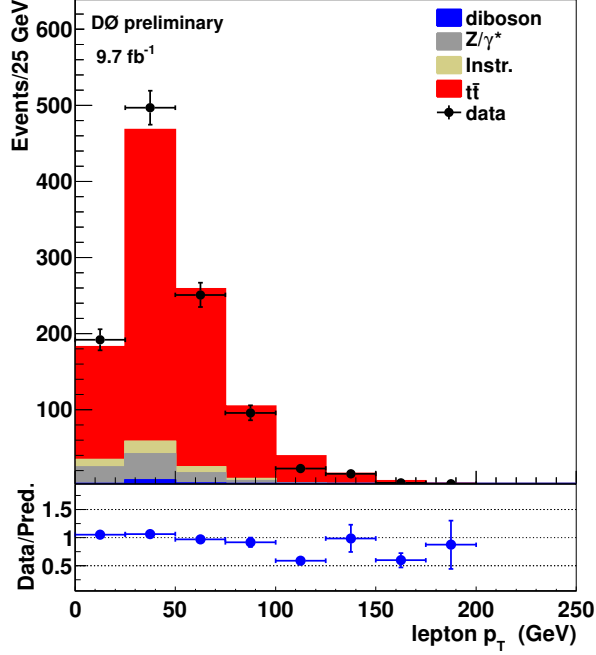


FIG. 2: Distributions in lepton  $p_T$  and data/prediction ratio for combined  $ee$ ,  $e\mu$  and  $\mu\mu$  channels, requiring at least two jets.

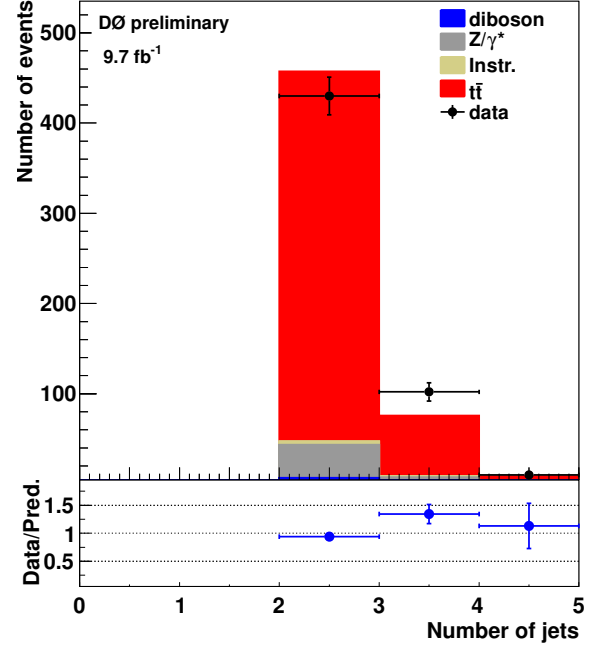


FIG. 3: Distribution in the number of jets and data/prediction ratio for combined  $ee$ ,  $e\mu$  and  $\mu\mu$  channels.

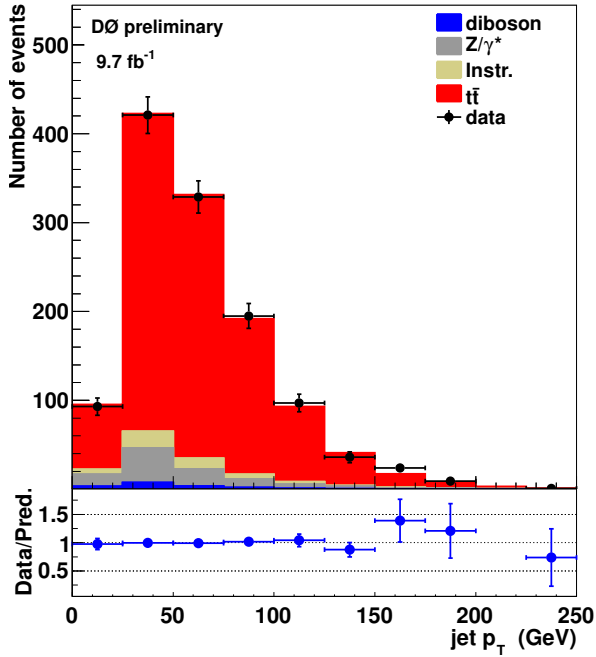


FIG. 4: Distributions in jet  $p_T$  after  $k_{JES}$  correction and data/prediction ratio for combined  $ee$ ,  $e\mu$  and  $\mu\mu$  channels, requiring at least two jets.

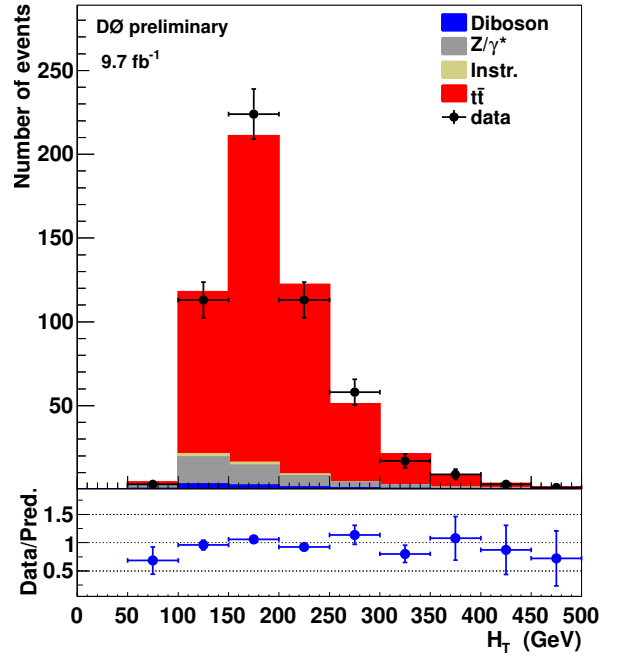


FIG. 5: Distributions in  $H_T$  after  $k_{JES}$  correction and data/prediction ratio for combined  $ee$ ,  $e\mu$  and  $\mu\mu$  channels, requiring at least two jets.

the processes  $q\bar{q} \rightarrow t\bar{t} \rightarrow W^+W^-b\bar{b} \rightarrow \ell^+\ell^-\nu_{\ell}\bar{\nu}_{\ell}b\bar{b}$  is used [42]. The matrix element  $\mathcal{M}$  is averaged over the colors and

spins of the initial state partons, and summed over the colors and spins of final state partons. The  $gg$  matrix element is ignored as it comprises only 15% of the total  $t\bar{t}$  production cross-section at the Tevatron, including it does not significantly improve the precision of the method. The term  $d\Phi_6$  represents the six-body phase space, and  $\sigma_{obs}(m_t)$  is the  $t\bar{t}$  cross section observed at the reconstruction level, calculated with the matrix element  $\mathcal{M}(y, m_t)$  and corrected for the selection efficiency.

The transfer functions  $W(x, y)$  describe the detector response to the reconstructed leptons and jets.

For this measurement, electron momenta and the directions of all reconstructed objects are assumed to be perfectly measured and are thus modelled with delta functions  $\delta(x - y)$ , reducing the dimensionality of the integration. This leaves the jet and muon momenta to be modelled.

Following the same approach as in the previous measurement [37], we parametrize the jet energy resolution as the sum of two Gaussian functions, with parameters depending linearly on parton energies, while the resolution in muon  $1/p_T$  is described by a single Gaussian function. All transfer function parameters are determined from simulated  $t\bar{t}$  events and updated for the final D0 object identifications [20, 24, 27] and final JES [12]. We use the same parametrizations for the transfer functions as in the  $\ell$ +jets top quark mass measurement, and their detailed description is given in Ref. [2].

The masses of the six final state particles are known, so we integrate over 8 dimensions in the  $ee$  channel, 9 dimensions in the  $e\mu$  channel and 10 in the  $\mu\mu$  channel. As integration variables we use the top and antitop quark masses, the  $W^+$  and  $W^-$  boson masses, the transverse momenta of the two jets,  $1/p_T$  for any muons and the  $p_T$  and  $\phi$  of the  $t\bar{t}$  system. This choice of variables is different from the previous measurement [37] and allows the reduction of the integration time by a factor of  $\sim 100$ .

To reconstruct the masses of the top quarks and  $W$  bosons, we solve the kinematic equations numerically and sum over the two possible jet-parton assignments and over all real solutions for each neutrino momentum [43]. If more than two jets exist in the event we use only the first two with highest transverse momenta. The integration is performed with the Monte Carlo based numerical integration algorithm VEGAS [44, 45], as implemented in the GNU Scientific Library (GSL) [46].

$Z/\gamma^*$  + jets events are the dominant source of background in the dilepton final state, (see Table 2), therefore we consider only the  $Z/\gamma^*$  + jets matrix element for the background probability calculation,  $P_{\text{bkg}}(x)$ . We use the LO  $Z/\gamma^* \rightarrow \ell\ell + 2\text{jets}$  ME from the VECBOS generator [47]. In the  $e\mu$  channel, the background events are produced by  $Z/\gamma^* \rightarrow \tau\tau \rightarrow \ell\ell + 2\text{jets}$  process. Since  $Z/\gamma^* \rightarrow \tau\tau$  decays are not implemented in VECBOS, we use an additional transfer function to describe the energy of the final state lepton relative to the initial  $\tau$  lepton, derived from parton-level information [43]. As for the case of the  $t\bar{t}$  probability, the jet and charged-lepton directions are assumed to be well-measured, and each kinematic solution is weighted according to the  $p_T$  of the  $Z/\gamma^*$  + jets system. The integration of  $P_{\text{bkg}}(x)$  is performed over the energies of the two jet partons and both possible assignments of jets to quarks.

The normalization of the background probabilities could be done in the same way as for the signal probabilities. However, the computation of the integral given by Eq. (4) requires significant computational resources, so a different approach is chosen. In this approach we minimize the difference between the fitted signal fraction and expected true fraction by adjusting the background normalization; see Ref. [48] for more details.

## B. Likelihood evaluation and $m_t$ extraction

In order to extract the top quark mass from a set of  $n$  events with measured four-momenta  $x_1, \dots, x_n$ , a log-likelihood function is built from the event probabilities

$$-\ln L(x_1, \dots, x_n; f_{t\bar{t}}, m_t) = -\sum_{i=1}^n \ln(P_{\text{evt}}(x_i; f_{t\bar{t}}, m_t)). \quad (5)$$

This function is minimized by adjusting two free parameters: the signal fraction,  $f_{t\bar{t}}$ , and the top quark mass,  $m_t$ . To calculate the signal probabilities, we use step sizes of 2.5 GeV for  $m_t$  and 0.004 for  $f_{t\bar{t}}$ . To fit the minimum value of the log-likelihood function,  $m_{\text{hood}}$ , we use a second degree polynomial function in the range of [-5 GeV, +5 GeV] around the minimum. The statistical uncertainty on the top quark mass,  $\sigma_{\text{hood}}$ , is given by the difference of the mass at  $-\ln L_{\text{min}}$  and  $-\ln L_{\text{min}} + 0.5$ .

## C. Method calibration

We calibrate the method, that is, correct for biases in the measured mass and statistical uncertainty, using an ensemble testing technique. We generate data-like ensembles with simulated signal and background events, measure

the top quark mass  $m_{\text{hood}}^i$  and uncertainty  $\sigma_{\text{hood}}^i$  in each ensemble  $i$  by the minimization of the log-likelihood function, and calculate the following quantities:

1. The mean value  $m_{\text{mean}}$  of the  $m_{\text{hood}}^i$  distribution. Comparison of the  $m_{\text{mean}}$  with the input to the simulation determines the mass bias.
2. The mean value  $\Delta m_t$  of the uncertainty distribution in  $\sigma_{\text{hood}}^i$ . This quantity characterizes the estimated uncertainty on the measured top quark mass from the log-likelihood fit.
3. The standard deviation of the pull variable distribution,  $w_{\text{pull}}$ , or pull width, where pull variable is defined as  $(m_{\text{hood}}^i - m_{\text{mean}})/\sigma_{\text{hood}}^i$ . The pull width provides a correction to the statistical uncertainty  $\sigma_{\text{hood}}$ .

We use a resampling procedure while generating the ensembles and apply a correction to account for it.

We use 500 ensembles per calibration point, with the number of events per ensemble equal to the number of events selected in data. In each ensemble the number of events from each background source is generated following a multinomial statistics, using the expected number of background events from Table 2. The number of  $t\bar{t}$  events is calculated as the difference between the total number of events in the ensemble and the generated number of background events. Using MC samples generated at five different top masses ( $m_{\text{MC}}$ ), we determine a linear calibration relation between the measured and generated masses:  $m_{\text{mean}} = p_0 + p_1(m_{\text{MC}} - 172.5)$ . The obtained curves for the combination of the three final states  $e\mu$ ,  $ee$  and  $\mu\mu$  are shown in Fig. 6.

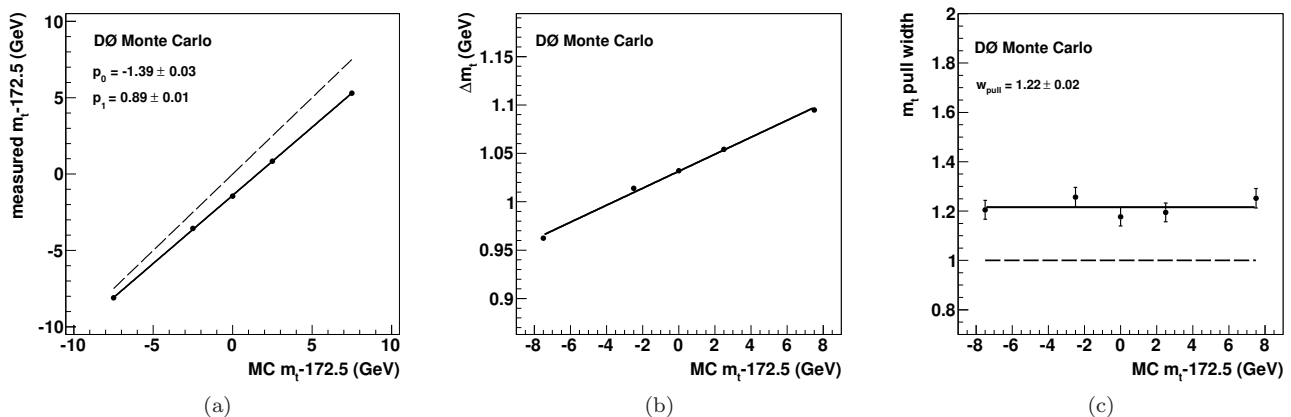


FIG. 6: The response of the ME method in  $m_t$  (a), the statistical uncertainty (b), and the pull width (c) for the combined  $ee$ ,  $e\mu$ ,  $\mu\mu$  channels.

The expected statistical uncertainty for the generated top quark mass 172.5 GeV is calculated as  $\sigma_{\text{exp}}(m_t) = \Delta m_t(172.5 \text{ GeV}) \cdot w_{\text{pull}}/p_1$ , and obtained values are presented in Table 3.

Final state	$ee$	$e\mu$	$\mu\mu$	$\ell\ell$
Uncertainty (GeV)	3.7	1.7	3.5	1.4

TABLE 3: The expected uncertainties in mass for the  $ee$ ,  $e\mu$ , and  $\mu\mu$  channels and combination.

## V. RESULT ON DATA

The fit to the data was performed using an unknown offset in the measured mass using the following steps. Only after the final approval of the methodology this offset was removed. Before performing the fit the  $k_{\text{JES}}$  JES correction factor from the lepton+jet mass analysis [1, 2] is applied to the jet  $p_T$  in data as  $p_T^{\text{corr}} = p_T/k_{\text{JES}}$ , independently for each data taking period. The correction procedure is explained in Section II. The uncertainties related to the propagation of this correction from  $\ell$ +jets to the dilepton final state are included in the systematic uncertainties budget as “residual JES uncertainty” and “statistical uncertainty on  $k_{\text{JES}}$  scale factor” in Section VI B 1. We apply the ME technique to data events as follows:

1. The log-likelihood function in data is shown in Figure 7.
2. The calibration correction from Fig. 6 is applied to  $m_{\text{lhood}}$  and  $\sigma_{\text{lhood}}$  to obtain the corrected measured values:

$$m_{\text{meas}} = (m_{\text{lhood}} - p_0 - 172.5 \text{ (GeV)})/p_1 + 172.5 \text{ (GeV)},$$

$$\sigma_{\text{meas}} = \sigma_{\text{lhood}} \cdot w_{\text{pull}}/p_1.$$

Table 4 shows the results for each channel separately and for the combination of the three channels. The distribution of the expected statistical uncertainty for the MC top quark mass 172.5 GeV and for the combination of the three channels  $ee$ ,  $e\mu$  and  $\mu\mu$  is shown in Figure 8.

Final state	$ee$	$e\mu$	$\mu\mu$	$\ell\ell$
$m_t$ (GeV)	$176.9 \pm 4.6$	$172.2 \pm 2.0$	$176.0 \pm 4.8$	$173.9 \pm 1.5$

TABLE 4: The measured top quark mass corrected for the calibration for  $ee$ ,  $e\mu$ ,  $\mu\mu$  channels, and for the combination of the three channels.

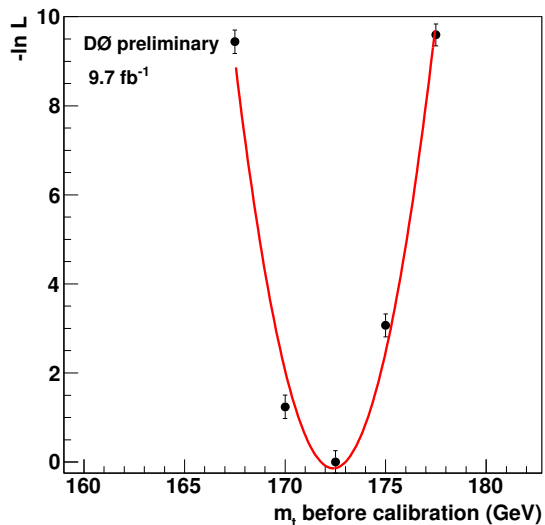


FIG. 7: The negative log-likelihood values for the observed data in dilepton channel as a function of generated top quark mass are fit to a quadratic in order to extract the (uncalibrated) measured mass. The range of the fit is  $\pm 5$  GeV around the minimum.

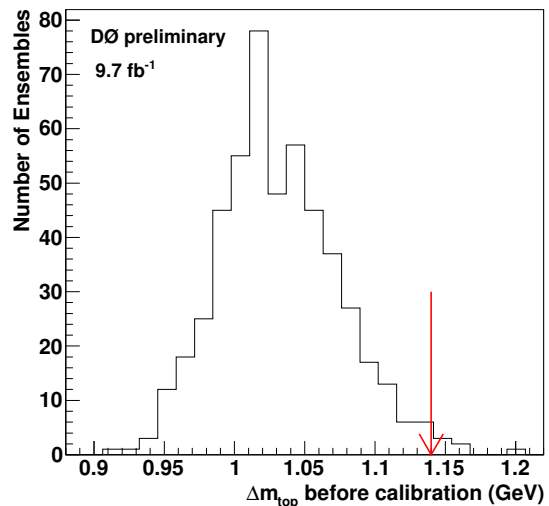


FIG. 8: Distribution of the expected statistical uncertainty  $\delta m_t$  (uncalibrated) for the combination of  $ee$ ,  $e\mu$  and  $\mu\mu$  channels and for the MC top quark mass 172.5 GeV. The arrow indicates the statistical uncertainty in data before calibration,  $\sigma_{\text{lhood}}$ .

## VI. SYSTEMATIC UNCERTAINTIES

Systematic uncertainties affect the measured  $m_t$  in two ways. First, the shape of the signal and background log-likelihood functions could be affected directly leading to the bias in the calibration curve. Secondly, the signal-to-background ratio in the selected data sample could be affected, leading to a different shape of the combined signal plus background log-likelihood function and to bias in the calibration curve. Ideally these two contributions would be treated coherently for each source of systematic uncertainty, but in practice the second effect is much smaller than the first for the most important systematic uncertainties. Therefore we keep the same signal-to-background ratio in pseudo-experiments except for the “signal fraction” systematic uncertainty. Background events are included in the evaluation of all sources of the systematic uncertainty. To derive all systematic uncertainties we use the simulated sample with  $m_t = 172.5$  GeV.

## A. Signal and background modeling systematic uncertainties

We determine uncertainties related to signal modeling by comparing simulations with different generators and parameters as described below. The evaluation of systematic uncertainties due to signal modeling follows the prescription used in  $\ell$ +jets ME analysis [2].

**Higher order corrections.** By default, we use ALPGEN to model our signal events, which is a LO generator. To evaluate the effect of higher order corrections on the top quark mass, we use signal events generated with MC@NLO. Because MC@NLO is interfaced to HERWIG for simulating the parton shower and hadronization, we use ALPGEN +HERWIG events for this comparison.

**Initial state radiation (ISR) and final state Radiation (FSR).** This systematic uncertainty is evaluated comparing the result using PYTHIA with the factorization and hadronization scale parameter varied by a factor  $\pm 50\%$  as done in Ref. [2].

**Hadronization and underlying event.** The systematic uncertainty due to the hadronization and underlying event models is estimated as the difference between the top quark mass measured using default ALPGEN +PYTHIA sample and samples with different hadronization models. We considered three alternative samples ALPGEN +HERWIG, ALPGEN +PYTHIA Perugia tune 2011C (with color reconnection), Perugia tune 2011NOCR (without color reconnection) [49]. We take the largest of these differences as an estimation of the systematic uncertainty on the hadronization and underlying event effects.

**Color reconnection.** We estimate the effect of the color reconnection model by comparing the top quark mass measured with ALPGEN +PYTHIA Perugia tune 2011C (with color reconnection) and Perugia tune 2011NOCR (without color reconnection) [49].

**$b$  quark fragmentation uncertainty ( $b$ -jet modeling).** Uncertainties in simulation of  $b$ -quark fragmentation can affect the  $m_t$  measurement through  $b$ -jet identification or transfer functions. This is studied using the procedure described in Ref. [50] by reweighting  $b$ -quark fragmentation to match a Bowler scheme tuned to either LEP or SLD data.

**PDF uncertainties.** The systematic uncertainty due to the choice of PDF is estimated by varying the 20 eigenvalues of the CTEQ6.1M PDF within their errors in the  $t\bar{t}$  MC. Ensemble tests are repeated for each of these changes and the total uncertainty is evaluated as in Ref. [2].

**Heavy-flavor scale factor.** In the ALPGEN  $Z \rightarrow \ell\ell$  + jets background samples, the fraction of heavy-flavor events is not well modelled. Therefore, a heavy-flavor scale factor is applied to the  $Z + b\bar{b}$  and  $Z + c\bar{c}$  cross sections to reproduce data. This scale factor has an uncertainty of  $\pm 20\%$ . We estimate its systematic effect by changing the scale factor up and down within this uncertainty.

**Transverse momentum of the  $t\bar{t}$  system.** The distribution of transverse momentum of  $t\bar{t}$  system was found not well modelled in  $\ell$ +jets. To evaluate this systematic uncertainty, we reconstruct the  $t\bar{t}$   $p_T$  from the two leading jets, two leading leptons, and  $\cancel{E}_T$ . The distribution in MC is reweighted to match that in data using a linear fit of  $t\bar{t}$   $p_T$ .

**Luminosity reweighting or multiple  $p\bar{p}$  interactions.** Multiple  $p\bar{p}$  interactions can potentially influence the measurement of  $m_t$ . By default, we reweight the luminosity profiles of our simulated MC samples to the luminosity profile found in data individually for each data taking epoch, before any selection requirements are applied. To estimate the possible mismatch in the luminosity profiles, we reweight the instantaneous luminosity profile in our MC to correspond to it in data after selection.

## B. Detector modeling uncertainties

### 1. JES systematic uncertainties

The relative difference between the JES in data and MC simulations is described by the global JES scale factor,  $k_{\text{JES}}$ , extracted from the  $\ell$ +jets mass measurement [1, 2]. As mentioned above, we apply this correction factor to jets  $p_T$  in data. In the previous  $5.4 \text{ fb}^{-1}$  dilepton analysis, the JES and  $b$ /light jet response were the dominant systematic uncertainties. The improvements made in the jet calibration [12] and the use of the  $k_{\text{JES}}$  factor in the dilepton channel reduce the uncertainty related to the JES from 1.5 GeV to 0.5 GeV.

**Residual jet energy scale uncertainty.** This uncertainty arises from the fact that the JES is jet  $p_T$  and  $\eta$  dependent. The determination of the JES correction in the  $\ell$ +jets measurement assumes a constant scale factor, i.e. we correct the average JES, but not the JES shape. Additionally, the  $k_{\text{JES}}$  correction could be affected by the different jet  $p_T$  requirements on jets in the  $\ell$ +jets and dilepton final states. There may also be a different JES offset correction due to the different jet multiplicities. We estimate these uncertainties as follows: we use MC samples in which the jet energies are shifted upward by one standard deviation of the  $\gamma$ +jet JES uncertainty. We correct jet  $p_T$  in these samples as  $p_T^{\text{corrMC}} = p_T^{\text{MC}} \cdot k_{\text{JES}}^{\text{UP}} / k_{\text{JES}}$ , where  $k_{\text{JES}}^{\text{UP}}$  is the JES correction measured in the  $\ell$ +jets analysis for

the MC samples shifted up by one standard deviation. This correction is applied separately for the each data taking period. The  $1/k_{\text{JES}}$  factor appears due the fact that  $k_{\text{JES}}$  is applied to the data samples and not to MC samples. The  $k_{\text{JES}}^{\text{DOWN}}$  is not measured in the  $\ell$ +jets final state, but assumed to have the same magnitude as the “UP variation.

**Uncertainty on  $k_{\text{JES}}$  factor.** The statistical uncertainty on the  $k_{\text{JES}}$  scale factor is 0.5% – 1.5% depending on the data taking epoch (Table 1). We recalculate the mass measured in MC for the  $k_{\text{JES}}$  correction shifted by one standard deviation. This procedure is applied individually for each data taking period, and the obtained uncertainties are summed up in quadrature.

**b/light jet response or flavor dependent uncertainty.** We apply this correction in our analysis and determine their uncertainty, to be about 0.5%. We shift the correction by the corresponding uncertainty up and down to determine the uncertainty in  $m_t$ .

## 2. Object reconstruction and identification

**Jet resolution systematic uncertainty.** The jet smearing, shifting, removing procedure [12] applies additional smearing to the MC jets, in order to account for the different jet  $p_T$  resolution in data and MC. To compute the systematic uncertainty on the jet resolution, the parameters of the jet energy smearing are varied by the size of the uncertainty.

**Electron momentum scale and resolution in energy.** This uncertainty reflects the difference in the absolute lepton momentum measurement and the simulated energy resolution [27] between data and MC. We vary the corresponding parameters by plus or minus one standard deviation for the simulated samples and assign the difference in the measured mass as a systematic uncertainty.

**Muon  $p_T$  resolution systematic uncertainty.** We vary the muon  $p_T$  resolution parameter [20] by  $\pm 1\sigma$  for the simulated samples and assign the difference in the measured mass as a systematic uncertainty.

**$b$ -tagging efficiency.** Difference in  $b$ -tagging modeling between data and simulation may cause systematic effects on  $m_t$ . To estimate this uncertainty, we vary the  $b$ -tagging corrections up and down within their uncertainties through reweighting.

**Trigger.** To evaluate the impact of trigger on our analysis we scale the number of background events according to the uncertainty on the trigger for different sub-channels. We rebuild ensembles according to the varied event fractions and rederive the mass. The number of signal  $t\bar{t}$  events is changed accordingly as the number of events in data minus the expected number of the background events.

**Jet identification.** Scale factors are used to correct the jet identification efficiency in MC. We estimate the systematic uncertainty by varying these scale factors by  $\pm 1\sigma$ .

## C. Method

**MC calibration.** The estimation of the statistical uncertainties due to the limited size of MC samples associated with the calibration procedure is obtained through the statistical uncertainty of the calibration curve parameters. To determine this contribution, we propagate the uncertainties on the calibration parameters  $p_0$  and  $p_1$  (Fig. 6) to  $m_t$ .

**Instrumental background.** To evaluate systematic uncertainty on instrumental background we vary its contribution up and down by 25%. The number of signal  $t\bar{t}$  events is changed accordingly as number of events in data minus number of the instrumental events and the ensembles tests are repeated with this configuration to extract  $m_t$ .

**Background contribution (or signal fraction).** To propagate the uncertainty associated to the background level, we vary the number of background events according to its uncertainty (see Table 2), rebuild ensembles, and rederive the mass. In the ensembles, the number of  $t\bar{t}$  events is defined as the observed number of events in data minus the expected number of background events.

**MC statistical uncertainty estimation.** To derive the MC statistical uncertainty in the  $t\bar{t}$  samples, we divide each sample into four independent subsets. The dispersion of masses from these subsets is used to estimate the uncertainty.

## D. Summary of systematic uncertainties

Table 5 summarizes all contributions to the uncertainty on the top mass measurement with the matrix element method. Each systematic source is scaled by  $1/p_1$  of  $m_t$  calibration curve from Fig. 6. The errors are symmetrized in the same way as in the  $\ell$ +jets measurement [1, 2]. We use sign  $\pm$  if the positive variation of the source of uncertainty corresponds to a positive variation of the measured mass, and  $\mp$  if it corresponds to a negative variation. As all

Source	Uncert. (GeV)
<i>Signal and background modeling:</i>	
Higher order corrections	+0.14
ISR/FSR	$\pm 0.16$
Hadronization & UE	+0.31
Color Reconnection	+0.13
$b$ -jet modelling	+0.21
PDF uncertainty	$\pm 0.20$
Heavy flavor	$\mp 0.06$
$p_T(t\bar{t})$	+0.03
Multiple $p\bar{p}$ interactions	-0.10
<i>Detector modeling:</i>	
Residual jet energy scale	-0.20
Uncertainty on kJES factor	$\mp 0.46$
Flavor dependent jet response	$\mp 0.30$
Jet energy resolution	$\mp 0.15$
Electron momentum scale	$\mp 0.10$
Electron resolution	$\mp 0.16$
Muon resolution	$\mp 0.10$
$b$ -tagging efficiency	$\mp 0.28$
Trigger	$\pm 0.06$
Jet ID	+0.04
<i>Method:</i>	
MC calibration	$\pm 0.03$
Instrumental background	$\pm 0.07$
MC background	$\pm 0.06$
Total systematic uncertainty	0.88
Total statistical uncertainty	1.51
Total uncertainty	1.75

TABLE 5: Summary of systematic and statistical uncertainties for the measurement of  $m_t$  in dilepton final states. The values are for the combination of  $ee$ ,  $e\mu$ , and  $\mu\mu$  channels.

the entries in the total systematic uncertainty are independent, the total systematic uncertainty on the top mass measurement is obtained by adding all the contributions in quadrature.

## VII. CONCLUSION

This note presents the D0 measurement of the top quark mass in dilepton final states, based on the matrix element technique for all Run II data corresponding to the integrated luminosity of  $9.7 \text{ fb}^{-1}$ . We measure the top quark mass

$$m_t = 173.9 \pm 1.5 \text{ (stat)} \pm 0.9 \text{ (syst)} \text{ GeV}$$

in agreement with the Tevatron and world average [3, 51]. This measurement significantly improves both statistical and systematic uncertainties of the previous dilepton matrix element measurement [37].

- 
- [1] V. M. Abazov *et al.* (D0 Collaboration), Precision measurement of the top-quark mass in lepton+jets final states, Phys. Rev. Lett. **113**, 032002 (2014).
  - [2] V. M. Abazov *et al.* (D0 Collaboration), Precision measurement of the top-quark mass in lepton+jets final states, Phys. Rev. D **91**, 112003 (2015).
  - [3] ATLAS Collaboration, CDF Collaboration, CMS Collaboration, and D0 Collaboration, First combination of Tevatron and LHC measurements of the top-quark mass (2014), arXiv:1403.4427.
  - [4] S. Abachi *et al.* (D0 Collaboration), Observation of the top quark, Phys. Rev. Lett. **74**, 2632 (1995).
  - [5] F. Abe *et al.* (CDF Collaboration), Observation of top quark production in  $p\bar{p}$  collisions, Phys. Rev. Lett. **74**, 2626 (1995).
  - [6] M. Jezabek and J. H. Kühn, Semileptonic Decays of Top Quarks, Phys. Lett. B **207**, 91 (1988).
  - [7] M. Jezabek and J. H. Kühn, QCD Corrections to Semileptonic Decays of Heavy Quarks, Nucl. Phys. **314**, 1 (1989).

- [8] V. M. Abazov *et al.* (D0 Collaboration), An Improved determination of the width of the top quark, *Phys. Rev. D* **85**, 091104 (2012).
- [9] W. Bernreuther, A. Brandenburg, Z. G. Si, and P. Uwer, Top quark pair production and decay at hadron colliders, *Nucl. Phys.* **690**, 81 (2004).
- [10] M. Czakon, M. L. Mangano, A. Mitov, and J. Rojo, Constraints on the gluon PDF from top quark pair production at hadron colliders, *J. High Energy Phys.* **1307**, 167 (2013).
- [11] V. M. Abazov *et al.* (D0 Collaboration), Precise measurement of the top quark mass in dilepton decays using optimized neutrino weighting, *Phys. Lett.* **B752**, 18 (2016).
- [12] V. M. Abazov *et al.* (D0 Collaboration), Jet energy scale determination in the D0 experiment, *Nucl. Instrum. Meth. A* **763**, 442 (2014).
- [13] V. M. Abazov *et al.* (D0 Collaboration), The upgraded D0 detector, *Nucl. Instrum. Meth. A* **565**, 463 (2006).
- [14] V. M. Abazov *et al.*, The muon system of the run II D0 detector, *Nucl. Instrum. Meth. A* **552**, 372 (2005).
- [15] M. Abolins *et al.*, Design and Implementation of the New D0 Level-1 Calorimeter Trigger, *Nucl. Instrum. Meth. A* **584**, 75 (2008).
- [16] R. Angstadt *et al.*, The Layer 0 Inner Silicon Detector of the D0 Experiment, *Nucl. Instrum. Meth. A* **622**, 298 (2010).
- [17] S. Ahmed *et al.*, The D0 Silicon Microstrip Tracker, *Nucl. Instrum. Meth. A* **634**, 8 (2011).
- [18] B. Casey *et al.*, The D0 Run IIb Luminosity Measurement, *Nucl. Instrum. Meth. A* **698**, 208 (2013).
- [19] V. Bezzubov *et al.*, The Performance and Long Term Stability of the D0 Run II Forward Muon Scintillation Counters, *Nucl. Instrum. Meth. A* **753**, 105 (2014).
- [20] V. M. Abazov *et al.* (D0 Collaboration), Muon reconstruction and identification with the Run II D0 detector, *Nucl. Instrum. Meth. A* **737**, 281 (2014).
- [21] G. C. Blazey *et al.*, in *Proceedings of the Workshop on QCD and Weak Boson Physics in Run II*, edited by U. Baur, R. K. Ellis, and D. Zeppenfeld (2000), pp. 47–77, hep-ex/0005012.
- [22] D. Bandurin, N. Bartosik, A. Das, G. Golovanov, Y. Ilchenko, A. Jayasinghe, R. Kehoe, H. Liu, G. Petrillo, Y.-T. Tsai, *et al.*, Jet Energy Scale Determination for D0 Run IIb (2012), D0 Note 6327.
- [23] V. M. Abazov *et al.* (D0 Collaboration), *b*-Jet Identification in the D0 Experiment, *Nucl. Instrum. Meth. A* **620**, 490 (2010).
- [24] V. M. Abazov *et al.* (D0 Collaboration), Improved *b* quark jet identification at the D0 experiment, *Nucl. Instrum. Meth. A* **763**, 290 (2014).
- [25] V. M. Abazov *et al.* (D0 Collaboration), Measurement of the  $t\bar{t}$  production cross section using dilepton events in  $p\bar{p}$  collisions, *Phys. Lett. B* **704**, 403 (2011).
- [26] V. M. Abazov *et al.* (D0 Collaboration), Measurement of the asymmetry in angular distributions of leptons produced in dilepton  $t\bar{t}$  final states in  $p\bar{p}$  collisions at  $\sqrt{s} = 1.96$  TeV, *Phys. Rev. D* **88**, 112002 (2013).
- [27] V. M. Abazov *et al.* (D0 Collaboration), Electron and Photon Identification in the D0 Experiment, *Nucl. Instrum. Meth. A* **750**, 78 (2014).
- [28] M. L. Mangano, M. Moretti, F. Piccinini, R. Pittau, and A. D. Polosa, ALPGEN, a generator for hard multiparton processes in hadronic collisions, *J. High Energy Phys.* **07**, 001 (2003).
- [29] T. Sjöstrand, S. Mrenna, and P. Z. Skands, PYTHIA 6.4 Physics and Manual, *J. High Energy Phys.* **05**, 026 (2006).
- [30] T. Affolder *et al.* (CDF Collaboration), Charged jet evolution and the underlying event in  $p\bar{p}$  collisions at 1.8 TeV, *Phys. Rev. D* **65**, 092002 (2002).
- [31] J. Pumplin *et al.*, New generation of parton distributions with uncertainties from global QCD analysis, *J. High Energy Phys.* **07**, 012 (2002).
- [32] P. M. Nadolsky *et al.*, Implications of CTEQ global analysis for collider observables, *Phys. Rev. D* **78**, 013004 (2008).
- [33] M. Czakon and A. Mitov, Top++: A Program for the Calculation of the Top-Pair Cross-Section at Hadron Colliders, *Comput.Phys.Comm.* **185**, 2930 (2014).
- [34] R. Brun and F. Carminati, Geant: Detector description and simulation tool, CERN Program Library Long Writeup W5013 (1993) (unpublished).
- [35] V. M. Abazov *et al.* (D0 Collaboration), Measurement of the  $t\bar{t}$  production cross section in  $p\bar{p}$  collisions at  $\sqrt{s} = 1.96$ -TeV using kinematic characteristics of lepton + jets events, *Phys. Rev.* **D76**, 092007 (2007).
- [36] V. M. Abazov *et al.* (D0 Collaboration), A precision measurement of the mass of the top quark, *Nature* **429**, 638 (2004).
- [37] V. M. Abazov *et al.* (D0 Collaboration), Precise measurement of the top quark mass in the dilepton channel at D0, *Phys. Rev. Lett.* **107**, 082004 (2011).
- [38] V. M. Abazov *et al.* (D0 Collaboration), Direct measurement of the mass difference between top and antitop quarks, *Phys. Rev. D* **84**, 052005 (2011).
- [39] T. Aaltonen *et al.* (CDF Collaboration), Measurement of the mass difference between top and antitop quarks, *Phys. Rev.* **D87**, 052013 (2013).
- [40] S. Chatrchyan *et al.* (CMS Collaboration), Measurement of the mass difference between top and antitop quarks, *JHEP* **06**, 109 (2012).
- [41] G. Aad *et al.* (ATLAS Collaboration), Measurement of the mass difference between top and anti-top quarks in pp collisions at  $\sqrt{s} = 7$  TeV using the ATLAS detector, *Phys. Lett.* **B728**, 363 (2014).
- [42] G. Mahlon and S. J. Parke, Maximizing spin correlations in top quark pair production at the Tevatron, *Phys. Lett. B* **411**, 173 (1997).
- [43] F. Fiedler, A. Grohsjean, P. Haefner, and P. Schieferdecker, The Matrix Element Method and its Application in Measure-

- ments of the Top Quark Mass, Nucl. Instrum. Meth. A **624**, 203 (2010).
- [44] G. Lepage, A new algorithm for adaptive multidimensional integration, Journal of Computational Physics **27**, 192 (1978).
  - [45] G. Lepage, Vegas: An adaptive multi-dimensional integration program (1980), Cornell preprint CLNS 80-447.
  - [46] M. Galassi, J. Davies, J. Theiler, B. Gough, G. Jungman, P. Alken, M. Booth, and F. Rossi, *GNU Scientific Library Reference Manual - Third Edition*, ISBN 0954612078 (Network Theory Ltd, 2009).
  - [47] F. A. Berends, H. Kuijf, B. Tausk, and W. T. Giele, On the production of a W and jets at hadron colliders, Nucl. Phys. **B357**, 32 (1991).
  - [48] A. Grohsjean, Measurement of the top quark mass in the dilepton final state using the matrix element method (2008), fermilab-Thesis-2008-92.
  - [49] P. Z. Skands, Tuning Monte Carlo Generators: The Perugia Tunes, Phys. Rev. D **82**, 074018 (2010).
  - [50] Y. Peters, K. Hamacher, and D. Wicke (D0 Collaboration), Precise tuning of the b fragmentation for the D0 Monte Carlo (2006).
  - [51] CDF and D0 collaborations, Combination of CDF and D0 results on the mass of the top quark using up to  $9.7 \text{ fb}^{-1}$  at the Tevatron (2014), arXiv:1407.2682.